Proceedings of the 2004 IEEE
International Conference on Robotics & Automation
New Orleans, LA • April 2004

A Dexterous System for Laryngeal Surgery

Multi-Backbone Bending Snake-like Slaves for Teleoperated Dexterous Surgical Tool Manipulation

Nabil Simaan, Russell Taylor
Johns Hopkins University-ERC-CISST
Baltimore, MD, 21218, USA
{nsimaan, rht}@cs.jhu.edu

Paul Flint
Johns Hopkins School of Medicine
Baltimore, MD, 21287, USA
pflint@jhmi.edu

Abstract— **This paper presents a design overview of a novel high DoF (Degrees-of-Freedom) system being developed for minimally invasive surgery of the throat. The system is designed to allow remote operation of 2-3 tools with high tip dexterity to enable suturing and soft-tissue manipulation while using the patient's mouth as the only entry port. The slave is a 34 DoF unit equipped with three snake-like distal dexterity units for surgical tool manipulation. Each of these units is a multi-backbone snake-like mechanism equipped with a detachable milli parallel manipulator allowing interchangeable tools to be used. The paper presents the outline of the kinematic analysis of the snake-like units and proposes one possible actuation redundancy resolution to allow further downsize scalability while reducing the risk of buckling of the primary backbone of the snake-like units. Finally, the paper presents a first early experiment with a prototype of the snake-like unit.**

Keywords- NiTi, multy backbone robot, snake robots, surgical assistant, master-slave mode.

I. INTRODUCTION

This paper reports our work to develop a high-dexterity robotic system for minimally invasive surgery (MIS) of the throat – an organ unusually challenging because of its shape, length, and complexity. Throat surgery is characterized by insertion of endoscopes and multiple long tools through a narrow tube (the laryngoscope) inserted into the patient's mouth. Current manual instrumentation is awkward, hard to manipulate precisely, and lacks sufficient dexterity to permit common surgical subtasks such as suturing vocal fold tissue. Our goal is a three-armed teleoperated robot with high distal dexterity capable of suturing and similar tissue manipulation tasks through the laryngoscope. Our approach emphasizes Distal Dexterity Units (DDU) with a novel design mounted on the end of precisely manipulated, thin robot arms. The DDU design is easily scalable to small sizes, simple to manufacture, and can be used with multiple detachable surgical tools.

Previous work on telerobotic systems for MIS has focused on endoscopic surgery of the chest and abdomen. The slave robots used in these systems use different mechanical architectures, including remote-center-of-motion mechanisms (e.g., [1], [2]), serial-link robots with passive joints [3], and mini-parallel robots (e.g., [4], [5]). Further examples may be found in [6]. A fundamental challenge for all of these robots is the kinematic constraint imposed by the passage of surgical tools through fixed entry ports into the patient's body. If more than four degrees-of-freedom (DoF) are required in manipulating a surgical instrument, then some form of distal dexterity mechanism is required.

Several approaches to distal tool dexterity enhancement have been reported. Many systems (e.g., [7] [2]) used wire actuated articulated wrists. Other systems used snake-like active bending devices. For example, [8] used bending SMA (Shape Memory Alloy) forceps for laparoscopic surgery. Dario *et al* [9] presented a 1 DoF SMA actuated a planar bending snake-like device for knee arthroscopy and [10] designed a hyper-redundant SMA actuated snake for gastro-intestinal intervention. Recently, [11] presented a two DoF 5 mm diameter wire-driven snake-like tool using super-elastic NiTi.

The authors of [7] analyzed alternative designs of a 3 DoF wrist for MIS suturing. They proposed a method to determine the workspace and to optimize the position of the entry port in the patient's body to provide optimal dexterity. More recently, [12] proposed an algorithm for entry port position optimization based on dexterity considerations. In throat surgery the entry port is predetermined (the patient's mouth) and multiple tools have to operate through a long and narrow laryngoscope. Hence, the need for extra dexterity and size reduction in MIS throat surgery is twofold.

In the current paper, we discuss our overall system design approach, but focus on our design for the DDU. The DDU differs from previous work in terms of application, size, downsize scalability, actuation, and kinematic architecture. In total, the DDU is equipped with seven actuated joints and has six independent DoF. The whole system presented in section III has 34 controlled DoF allowing the manipulation of up to three tools inside the throat.

The following section presents the clinical relevance of the chosen application of this system. Then, section III presents the overall system architecture. Section IV presents the workspace and force requirements from the designed system. Section V presents the distal dexterity units. Section VIII presents a kinematic analysis of the snake-like units. Section VII proposes a methodology for antagonistic actuation the downsize scalability of these snake-like units to even smaller diameters than 4 mm. VIII presents a first prototype of the snake-like unit of the DDU.

II. CLINICAL RELEVANCE

The human larynx, or voice box, is responsible for breathing, airway protection during swallowing, and voice

production. As with any organ system in the body, the larynx is subject to a variety of benign and malignant diseases requiring surgical procedures for excision and/or reconstruction. These procedures may be performed using open surgical techniques, or minimally invasive endoscopic procedures. Open procedures provide adequate exposure for excision and reconstruction at the expense of disrupting the framework supporting laryngeal cartilage, muscle and connective tissue vital to normal function. Endoscopic procedures preserve the laryngeal framework and provide a means for removal of tissue, however, functional reconstruction is not possible due to limited accessibility.

Regardless of the approach undertaken, preservation of the basic functions is paramount to maintaining quality of life. To maintain the voice characteristics, it is of prime importance to reconstruct the vocal fold structures as accurately as possible. Approaching these regions by using minimally invasive approach requires the use of an array of long MIS tools and a laryngoscope that is inserted into the patient's mouth and serves as a visualization tool and a guide for surgical instrumentation, Fig. 1. This surgical setup requires the surgeon to manipulate several long tools (for example one tool for suction and another for tissue manipulation) through a laryngoscope having an oval cross-section usually ranging between 16-20 mm in width.

The current array of MIS tools available for these surgeries does not provide the surgeons with the required tip dexterity to allow tissue flap rotation or sewing actions. The system presented in the following section is being designed and constructed to overcome these shortcomings.

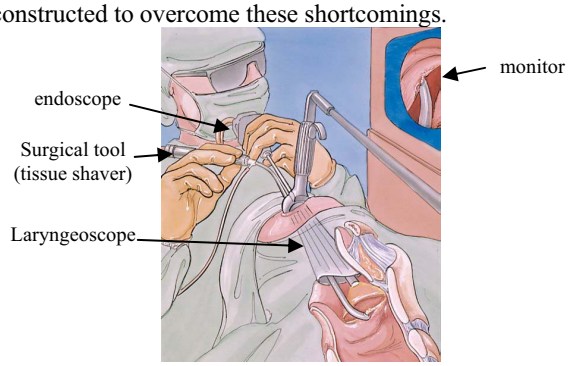

Fig. 1 A typical surgical setup of minimally invasive laryngeal surgery.

III. Overall System Architecture

Fig. 2 illustrates our throat surgery system. It includes a laryngoscope, a base link, two similar DDUs for tool/tissue manipulation, and another DDU for suction. Each DDU is mounted on a corresponding DDU holder, which is manipulated by a corresponding 4 DoF tool manipulation unit (TMU) that controls the angle of approach, the rotation about and the position along the axis of the DDU holder. The TMUs are mounted on a rotating base unit (RBU) permitting the system to be oriented within the throat so as to minimize collisions between DDU holders. The DDU holders are thin tubes (about 4 mm in outside diameter) providing an actuation pathway for the DDU and possibly a light-source or a suction channel. Each TMU is equipped with a fast clamping device allowing the surgeon to adjust the axial location of the DDU. The actuation unit of each DDU is located at the upper extremity of each tool and the actuation is by super-elastic tubes operated in push-pull mode as described in section V.

Excluding the degrees of freedom associated with the distal dexterity units, this system has thirteen controlled degrees of freedom. Each DDU adds seven controlled actuators to produce 6 DoF motion, as presented in section V. Hence, the total slave system of Fig. 2 has thirty four controlled actuators.

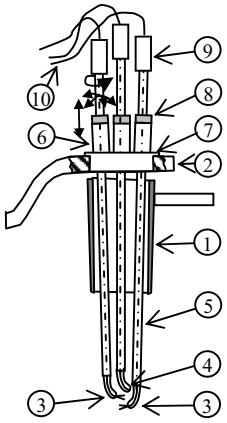

1 laryngoscope
2 base link
3 Distal dexterity unit
4 suction snake
5 DDU holder
6 4 DoF tool manipulation unit (TMU)
7 rotating base
8 fast clamping device
9 DDU actuation unit
10 electrical supply /data

Fig. 2 Overview of the throat surgical assistance slave.

IV. Clinical Workspace and Force Requirements

The clinical application defines the required workspace and force application capability of the system. The goal reachable workspace for tele-operated suturing past and in the vicinity of the vocal folds requires a cylindrical work volume 40 mm in diameter and 50 mm in height. This defines a conservative required workspace for the TMUs manipulating the DDU holder. Also, the length of the DDU holder is enough to reach 180-250 mm into the throat. The requirement from the DDU is to be able to bend 90° sideways in any direction and to transmit rotation of the DDU holder about its axis into rotation about the axis of the gripper. This feature will be used for the suturing application. The required force application capability is 1 newton at the tip of the gripper for tissue manipulation.

V. The Distal Dexterity Units

Fig. 3 presents the distal dexterity unit composed of a bending snake-like unit and a detachable "milli-parallel" wrist. The distal dexterity units provide the necessary flexibility for bypassing obstacles and delivering torque about their backbone thus transforming the rotation of the snake holder about its axis into rotation of the snake-like unit about its backbone axis. This is a valuable property for suturing and tissue manipulation in a confined space. This section presents these units in detail.

A. The multi-backbone snake-like unit

Snake-like robots can be classified based on their backbone characteristics and according to their actuation. TABLE I. presents this classification and summarizes some of

the works in this field. As in the table, snake like robots can be classified into discrete or continuous backbone robots and into extensible or non-extensible backbone robots. Also, they can be classified according to their actuation into continuous actuation or binary actuation robots. Robots with discrete backbones use a serial chain backbone made of rigid bodies and joints while continuous backbone robots use a flexible material (such as an elastomer, a spring, bellows, or a flexible thin rod) as a backbone. Robots with extensible backbones can change the overall length of their backbone. The snake-like unit presented here is a continuous non-extensible multi-backbone unit.

The snake-like unit is composed from a base disk, an end disk, several spacer disks, and four super-elastic tubes arranged as in Fig. 3. These tubes are called the backbone tubes of this snake-like unit. The central tube is the *primary backbone* while the remaining three tubes are the *secondary backbones*. The secondary backbones are equidistant from the central backbone and from one another. The central backbone is attached to both the base and end disks and to all spacer disks while the secondary backbones are attached only to the end disk and are free to slide and bend through properly dimensioned holes in the base and spacer disks. These secondary backbones are used for actuating this snake-like device and they pass through guiding channels in the DDU holder to allow their actuation in both push and pull modes. The spacer disks are distanced from one another to prevent buckling of the central and secondary backbones and to maintain an equal distance between the secondary backbones and the central backbone.

This design is inspired by the works of [19] and [16], who suggested and analyzed the kinematics and internal statics of wire-actuated flexible backbone (continuum) robots. Using the terminology of [19] and [16], the snake-like unit of Fig. 3 represents one bending 'section' in a snake robot. Using additional super-elastic tubes passing through the secondary backbones of a first section, allows serial stacking of a second section. This opens the possibility of multi-section snake that can be used for exploration and surgical intervention in deeper regions through the lung airways.

The key difference between this design and these works ([19], [16]) is in the size and in the use of secondary backbones that have the same size as the primary backbone and therefore their bending properties are significant (i.e. they can not be treated as wires). This is important when designing small diameter snake-like robots while maintaining structural rigidity and simplicity of actuation.

By using three push-pull elements for the actuation of the snake-like unit of Fig. 3 it is possible to satisfy the statics of the structure while preventing buckling of the backbones – an important feature for the successful reduction of diameter for medical applications requiring smaller diameter than 4 mm.

One architecture-inherent advantage of the snake-like unit of Fig. 3 stems from using flexible backbones, thus removing the dependency on small universal joints and wires. This reduces the manufacturing costs of the unit and contributes to the possible reduction in its size due to the small number of moving parts and the absence of standard miniature joints. Another advantage comes from the use of tubes for the backbones, thus providing a secondary application for these backbones. These backbones can serve also as suction channels, actuation channel for the tool mounted on its distal end or as a source of light for imaging.

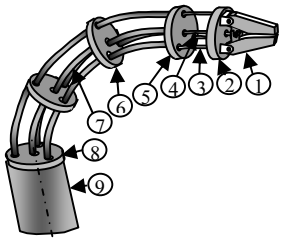

1 gripper
2 moving platform
3 parallel stage wires
4 gripper wire
5 end disk
6 spacer disk
7 central backbone tube
8 base disk
9 DDU holder

Fig. 3 The DDU (Distal Dexterity Unit) using a multi-backbone snake-like robot with detachable parallel tip.

TABLE I. ARCHITECTURE PROPERTIES OF SNAKE LIKE ROBOTS IN PREVIOUS WORKS.

Sample works	Classification criteria					
	Backbone architecture		*Backbone extensibility*		*Actuation*	
	discrete	*continuous*	*extensible*	*Non extensible*	*continuous*	*discrete*
[13], [14],[15], [16]	●			●	●	
[17], [18]	●		●			●
[19], [20]		●		●	●	
[21][22],[23]		●	●		●	

B. *The detachable milli-parallel unit*

The snake-like unit described in the preceding section is capable for providing two DoF for the distal tip of the MIS tool. These DoF are associated with bending sideways in any direction. However, this unit is of reduced applicability if it is equipped only with one tool (i.e., grippers) since the surgical applications requires different gripper geometries and different tools. Hence, an efficient way to attach different tools to the snake-like unit is required. To achieve this, a milli-parallel unit is being constructed. This unit will not only answer the need for tool detachability, but will also provide additional three DoF for delicate and accurate motions in a very confined space; thus utilizing the architecture-inherent rigidity of parallel robots and supporting further downsize scalability of the DDU while maintaining useful structural rigidity.

The detachable milli-parallel unit is constructed from super-elastic actuation wires passing through the secondary backbones, spherical joints, and a moving platform to which a gripper of a tool is affixed, Fig. 4. The moving platform is machined with matching groves such that the balls attached to the end of the actuation wires match its diameter and a flexible locking ring is placed around the circumference of the moving platform to maintain these balls inside their grooves. To detach the tool one needs to remove the ring and remove the moving platform together with its gripper/tool.

There are two possible operation modes using the detachable milli-parallel unit. In the first mode of operation, the actuation wires are used only to extend outwards in order to attach a new moving platform equipped with another tool. Once the tool is attached then the actuation wires are retrieved until the moving platform is secured on the end platform of the snake-like unit. In the other mode, for operations requiring small workspace and fine motions, the actuation wires are used to actuate the moving platform as a three DoF parallel platform with extensible links. The flexibility of the wires allows the motion of the moving platform even though the actuation wires maintain perpendicularity to the end disk of the snake-like unit through their passage ports.

The actuation wire for the gripper/tool is also equipped with a fast connection to the gripper and is extended according to the kinematics of the DDU to maintain the operation of the tool. This wire can also be used for micro-drill applications where it is also actuated in rotation.

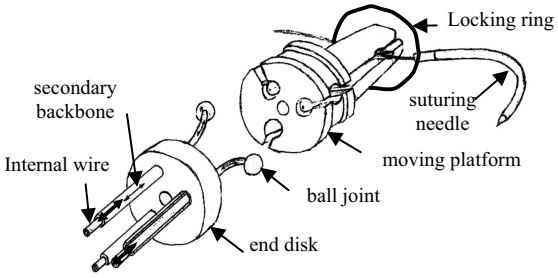

Fig. 4 The detachable parallel tip.

VI. KINEMATICS OF THE SNAKE-LIKE UNIT

This section presents the instantaneous kinematics of the snake-like unit. By controlling the lengths of the secondary backbones, the end disk is moved in two DoF in space. The snake-like unit assumes a shape that minimizes its potential energy. This shape is given by shape functions that are a solution of a system of non-linear partial differential equations [20] [19]. A general closed-form solution has not been obtained and some simplifying assumptions are necessary to obtain the approximate shape of the backbones. The following list summarizes the simplifying assumptions made in this paper.

1. The weight of the disks of the snake-like unit is negligible. Hence, the snake unit bends in a plane perpendicular to the base disk once the secondary backbones are actuated. This is not true for large snake-like robots [19] since gravity can change the minimum potential energy solution.
2. The external forces acting on the DDU are small enough not to considerably change the overall potential energy of the system, i.e., the forces are small enough to cause small deflections from the nominal kinematic solution.
3. The spacer disks are placed close enough to each other so that the shapes of the primary and secondary backbones are constrained to lie a prescribed fixed distance apart.
4. The shape of the central backbone is assumed to be a continuous smooth function parameterized by the radius of curvature $\rho(s)$. This is true only if the spacer disks are designed and fixed on the primary backbone such that they do not prevent it from bending while providing negligible friction.

A. Kinematic nomenclature

Fig. 5 shows the snake-like unit in a bent configuration with only the primary and one secondary backbone illustrated. Three coordinate systems are also shown. These coordinate systems are the Base Disk coordinate System (BDS) $\{\hat{\mathbf{x}}_b\ \hat{\mathbf{y}}_b\ \hat{\mathbf{z}}_b\}$, the Snake Plane coordinate System (SPS) $\{\hat{\mathbf{x}}_1\ \hat{\mathbf{y}}_1\ \hat{\mathbf{z}}_1\}$, and the End Disk coordinate System (EDS) $\{\hat{\mathbf{x}}_e\ \hat{\mathbf{y}}_e\ \hat{\mathbf{z}}_e\}$. BDS is attached to the base disk such that $\hat{\mathbf{x}}_b$ points from the center to the first secondary backbone and $\hat{\mathbf{z}}_b$ is normal to the disk as in Fig. 5. $\hat{\mathbf{z}}_1$ is perpendicular to the base disk and $\hat{\mathbf{x}}_1$ lies along the intersection of the snake plane (the plane in which the snake unit bends) and the base disk. EDS is obtained from SPS by a simple rotation about $\hat{\mathbf{y}}_1$ such that $\hat{\mathbf{z}}_1$ becomes the backbone tangent at the end disk. The following symbols are defined:

- i - index of the secondary backbones i=1,2,3.
- s - arc-length parameter of the primary backbone. s=0 at the base disk and s=L at the end disk.
- L_i - length of the i^{th} backbone from the base to the end disk.
- r - radius of the base, spacer, and end disks.
- $\rho(s)$ - radius of curvature defined as $\left|ds/d\theta(s)\right|$.
- $\theta(s)$ - the angle of the primary backbone tangent in the $\hat{\mathbf{x}}_1\ \hat{\mathbf{z}}_1$ plane. $\theta(s=L)$ and $\theta(s=0)$ are designated by θ_L and θ_0, respectively.
- δ_i - the right-handed rotation angle from $\hat{\mathbf{x}}_1$ about $\hat{\mathbf{z}}_1$ to a line passing through the primary backbone and the i'th secondary backbone at s=0.
- δ - the snake plane angle. It is defined as $\delta = \delta_1$.
- β - division angle ($\beta = 2\pi/n$ where n is the number of secondary backbones).
- $\dot{x}$ - time derivative of variable x.
- $\mathbf{J}_{xy}$ - Jacobian matrix such that $\dot{\mathbf{x}} = \mathbf{J}\dot{\mathbf{y}}$. The only exception for this nomenclature is $\mathbf{J}_{\omega x}$, which represents the mapping $\boldsymbol{\omega} = \mathbf{J}_{\omega x}\dot{\mathbf{x}}$ where $\boldsymbol{\omega}$ is an angular velocity.

B. Kinametic relations between the backbones

The position and orientation of the end disk relative to the base disk is characterized by two angles θ_L and δ. The angles δ_i i=1,2,3, are related to δ according to Eq. (1), Fig. 5.

$$\delta_i = \delta + (i-1)\beta, \quad i = 1,2,3 \tag{1}$$

The projection of the i'th secondary backbone on the snake plane is a curve which is offset by $\Delta_i \in [r, -r]$ from the primary backbone. The radius of curvature and arc-length of this curve are respectively indicated by s_i and $\rho_i(s_i)$ and are related to the parameters of the primary backbone according to Eq. (2).

$$\rho(s) = \rho_i(s) + \Delta_i, \text{ where } \Delta_i \equiv r\cos(\delta_i),\ \theta_L \in [0, \theta_0] \tag{2}$$

The length of the primary backbone and the length of the i^{th} backbone are related according to:

$$L_i = \int ds_i = \int ds_i - ds + ds = L + \int_{\theta_L}^{\theta_0} \left(\rho_i(s) - \rho(s)\right) d\theta \quad \theta_L \in [0, \theta_0] \quad (3)$$

Using Eq. (2), yields the interesting result of Eq. (4). The length of the i'th backbone depends on the angle of the end disk relative to the base disk. It does not depend on the shape of the backbone (see also [19]).

$$L_i = L + \Delta_i(\theta_L - \theta_0) \qquad \theta_L \in [0, \theta_0] \quad (4)$$

C. Direct kinematics

Given the lengths of the primary backbone and of two secondary backbones, one seeks the length of the third secondary backbone and the configuration of the end disk. Assume that L_1 and L_2 are given, then Eq. (4) results in the end disk angle θ_L as a function of an unknown offset Δ_i.

$$\theta_L = \theta_0 - \left(L - L_i\right)/\Delta_i \quad (5)$$

Using Eqs. (1, 2, 4) and some trigonometric manipulation, one can write a kinematic compatibility condition on L_1 and L_2:

$$\underbrace{\left[\left(L - L_1\right)c_\beta - \left(L - L_2\right)\right]}_{A} c_{\delta 1} - \underbrace{\left[\left(L - L_1\right)s_\beta\right]}_{B} s_{\delta 1} = 0 \quad (6)$$

where c_x and s_x stand for the cosine and sine of angle x.

Solving for $\delta=\delta_1$ results in two solutions of Eq. (7) for whom the corresponding solutions for θ_L were given in Eq. (5). These two solutions represent the same one possible configuration of the snake, but for two opposing directions of $\hat{x}_1$ of Fig. 5.

$$\delta = \text{Atan2}(A/B) \quad \text{or} \quad \text{Atan2}(A/B) + \pi \quad (7)$$

The required length of the third backbone is found by using Eq. (5) for the value of δ given by Eq. (7).

The position, $\mathbf{p}_L$, and the orientation, ${}^b\mathbf{R}_e$, of the end disk are found by integrating along the tangent of the backbone and by a successive rotation sequence as in Eq. (8). The matrix ${}^b\mathbf{R}_1$ is a rotation matrix of $(-\delta)$ about $\hat{\mathbf{z}}_b$ and ${}^1\mathbf{R}_e$ is a rotation matrix of $(\theta_0 - \theta_L)$ about $\hat{\mathbf{y}}_1$, Fig. 5.

$$\mathbf{p}_L = {}^b\mathbf{R}_1 \left[\int_0^L \cos(\theta(s))\, ds, 0, \int_0^L \sin(\theta(s))\, ds\right]^t, \quad {}^b\mathbf{R}_e = {}^b\mathbf{R}_1\, {}^1\mathbf{R}_e \quad (8)$$

D. Instantaneous kinematics

This section presents the mapping between the actuation speeds $\dot{\mathbf{q}} \equiv [\dot{L}_1, \dot{L}_2]^t$ and the generalized twist of the end disk, $\dot{\mathbf{x}}$. The generalized twist is denoted by a 6×1 vector $\dot{\mathbf{x}} = \left[\dot{\mathbf{p}}_L{}^t, \boldsymbol{\omega}_L{}^t\right]^t$ where $\dot{\mathbf{p}}_L$ and $\boldsymbol{\omega}_L$ designate the linear and angular velocity of the end disk. In this section, we would like to find the Jacobian $\mathbf{J}_{xq}$. The section proceeds without giving all the explicit expressions for space limitations. This section follows similar methods as in [14], [19].

$$\dot{\mathbf{x}} = \mathbf{J}_{xq}\, \dot{\mathbf{q}} \quad (9)$$

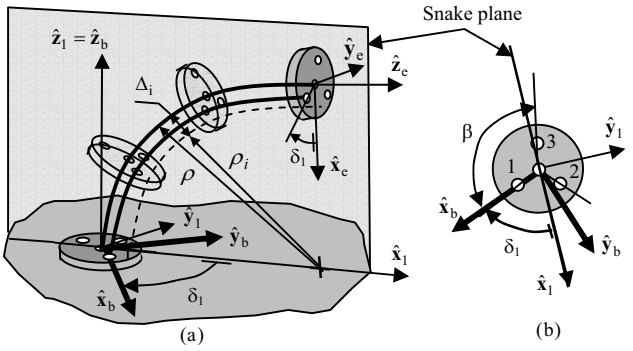

Fig. 5 The snake-like unit in a bent configuration (a) top v iew of the base disk (b)

If the snake unit is actuated by three secondary backbones, then it is assumed that the third backbone fulfills the kinematic constraint of Eq. (6) at all times.

The angular velocity of the end disk is given by $\boldsymbol{\omega}_{e/b}$:

$$\boldsymbol{\omega}_{e/b} = -\dot{\delta}\, \hat{\mathbf{z}}_1 - \dot{\theta}_L\, \hat{\mathbf{y}}_1 \quad (10)$$

By defining $\dot{\boldsymbol{\psi}} \equiv \left[\dot{\theta}_L, \dot{\delta}\right]^t$ and taking the time derivative of Eq. (6), one finds the Jacobian relating the joint speeds with the elements of the end disk angular velocity:

$$\dot{\boldsymbol{\psi}} = \begin{bmatrix} \mathbf{J}_{\theta_L q} \\ \mathbf{J}_{\delta q} \end{bmatrix} \dot{\mathbf{q}} = \mathbf{J}_{\psi q} \dot{\mathbf{q}}, \quad \mathbf{J}_{\psi q} \equiv \begin{bmatrix} \mathbf{J}_{\theta_L q} \\ \mathbf{J}_{\delta q} \end{bmatrix} \quad (11)$$

where $\mathbf{J}_{\theta_L q}, \mathbf{J}_{\delta q} \in \Re^{1\times 2}$ represent the mappings $\dot{\theta} = \mathbf{J}_{\theta_L q}\dot{\mathbf{q}}$, $\dot{\delta} = \mathbf{J}_{\delta q}\dot{\mathbf{q}}$. By using Eq. (11) one obtains the angular velocity.

$$\boldsymbol{\omega}_{e/b} = \mathbf{J}_{\omega\psi}\dot{\boldsymbol{\psi}} = \mathbf{J}_{\omega\psi}\mathbf{J}_{\psi q}\dot{\mathbf{q}} = \mathbf{J}_{\omega q}\dot{\mathbf{q}} \quad (12)$$

The shape of the backbone is a function of θ_L and $\theta(s) = f(\theta_L, s)$. By taking the time derivative of this function one obtains a distribution of bending speed along the backbone as a function of the bending speed of the tip. This distribution is designated by $g(\theta_L, s)$, Eq. (13).

$$\dot{\theta}(s) = \frac{\partial f}{\partial \theta_L}\frac{\partial \theta_L}{\partial t} + \frac{\partial f}{\partial s}\underbrace{\frac{\partial s}{\partial t}}_{0} = g(\theta_L, s)\, \dot{\theta}_L \quad (13)$$

The linear velocity of the end disk in SPS is given by:

$${}^1\dot{\mathbf{p}}_L = \dot{\theta}_L \left[\left(\int_0^L -\sin(\theta(s))\, g(\theta_L, s)\, ds\right), 0, \left(\int_0^L \cos(\theta(s))\, g(\theta_L, s)\, ds\right)\right]^t \quad (14)$$

The linear velocity of the end disk relative to the base is:

$$\dot{\mathbf{p}}_L = {}^b\mathbf{R}_1 \left({}^1\dot{\mathbf{p}}_L + \boldsymbol{\omega}_{1/\text{base}} \times {}^1\mathbf{p}_L\right) \quad (15)$$

where $\boldsymbol{\omega}_{1/\text{base}} = -\dot{\delta}\hat{\mathbf{z}}_b$ is the angular velocity of SPS in BDS. These results lead to the following Jacobian mapping:

$$\dot{\mathbf{p}}_L = \mathbf{J}_{p\psi}\dot{\boldsymbol{\psi}} = \mathbf{J}_{p\psi}\mathbf{J}_{\psi q}\dot{\mathbf{q}} = \mathbf{J}_{pq}\dot{\mathbf{q}} \quad (16)$$

Hence, the Jacobian of the snake unit is given by:

$$\dot{\mathbf{x}} = \begin{bmatrix} \mathbf{J}_{pq} \\ \mathbf{J}_{\omega q} \end{bmatrix} \dot{\mathbf{q}} = \mathbf{J}\,\dot{\mathbf{q}}, \Rightarrow \quad \mathbf{J}_{xq} = \begin{bmatrix} \mathbf{J}_{pq} \\ \mathbf{J}_{\omega q} \end{bmatrix} \quad (17)$$

These results depend on the shape function, $\theta(s)$, minimizing the potential energy of the system. For ideal unloaded snake-like unit $\theta(s)$ will be a circular section of length L [19]. Otherwise, numerical or direct variational methods can be used to find an approximation for $\theta(s)$.

VII. Antagonistic Actuation

The snake-like unit of Fig. 3 has one redundant secondary backbone. This backbone can be actuated to reduce the amount of force acting on the primary backbone and by doing so, reducing the risk of its buckling. This section presents a redundancy resolution that achieves this goal. This feature is important to allow effective downsize scalability while preventing the thin primary backbone from buckling. The analysis is based on a linearized virtual work model in which the effects of actuation forces on the total deformation energy of the backbones is negligible compared to the total deformation energy due to the bending of the backbones. Under this assumption, the energy of the system of backbones is a function of the bending of the backbones. Since the shape is characterized by $\theta(s) = f(\theta_L, s)$ and δ, the energy may be presented as a function of $\theta(s) = f(\theta_L, s)$ and δ.

$$E = E(\theta_L, \delta) \tag{18}$$

Assume an external wrench $\mathbf{w}_e = \left[\mathbf{f}_e{}^t, \mathbf{m}_e{}^t\right]^t$ is acting on the end disk where $\mathbf{f}_e$ indicates the force and $\mathbf{m}_e$ the moment. The virtual work principle is used by assuming a change in the posture of the end disk, $\Delta\mathbf{x}$, an external wrench, $\mathbf{w}_e$, acting on the end-disk, a corresponding change in the secondary backbones' lengths, $\Delta\mathbf{L} \equiv [\Delta L_1, \Delta L_2, \Delta L_3]^t$, and an associated actuation forces, $\boldsymbol{\tau} \equiv [\tau_1, \tau_2, \tau_3]^t$, and a change in the potential energy of the backbone system ΔE, Eq. (19).

$$\mathbf{w}_e{}^t \Delta\mathbf{x} + \boldsymbol{\tau}^t \Delta\mathbf{L} - \Delta E = 0 \tag{19}$$

The virtual displacement of the snake unit is characterized by $\Delta\boldsymbol{\psi} = [\Delta\theta_L, \Delta\delta]^t$. The entities $\Delta\mathbf{x}$ and $\Delta\mathbf{L}$ are related to $\Delta\boldsymbol{\psi}$ according to Eqs. (20).

$$\Delta\mathbf{L} = \mathbf{J}_{L\psi}\Delta\boldsymbol{\psi} \qquad \Delta\mathbf{x} = \mathbf{J}_{x\psi}\Delta\boldsymbol{\psi} \tag{20}$$

where $\mathbf{J}_{x\psi}$ is given by Eq. (21) and $\mathbf{J}_{L\psi}$ is found by taking the time derivative of Eq. (4) for L_i, i=1,2,3.

$$\mathbf{J}_{x\psi} = \begin{bmatrix} \mathbf{J}_{p\psi} \\ \mathbf{J}_{\omega\psi} \end{bmatrix} \tag{21}$$

Next, the virtual work principle is rewritten as in Eq. (22). The equilibrium condition requires the terms associated with each independent DoF to vanish. This results in a system of two equations in three unknowns $\boldsymbol{\tau} \equiv [\tau_1, \tau_2, \tau_3]^t$. The matrix for of this system of equations is given in Eq. (23) where ∇E represents the gradient of the potential elastic energy.

$$\mathbf{w}_e{}^t \mathbf{J}_{x\psi}\Delta\boldsymbol{\psi} + \boldsymbol{\tau}^t \mathbf{J}_{L\psi}\Delta\boldsymbol{\psi} - [\nabla E]^t \Delta\boldsymbol{\psi} = 0 \tag{22}$$

$$\mathbf{J}_{L\psi}{}^t \boldsymbol{\tau} = \nabla E - \mathbf{J}_{x\psi}{}^t \mathbf{w}_e \tag{23}$$

Eq. (23) is a system of two equations in three unknowns. An additional requirement is necessary to choose among the infinite number of solutions. This requirement is minimizing the total force on the primary backbone such that the resultant force on it is zero, Eq. (24). This means that the actuation forces balance the external force and that there are only moments acting on the primary backbone. In a simplified approach, the secondary backbones will assume the same direction given by $\hat{\mathbf{z}}_e$ (Fig. 5).

$$\mathbf{Z_e}\ \boldsymbol{\tau} = -\mathbf{f}_e, \quad \text{where} \quad \mathbf{Z_e} \equiv [\hat{\mathbf{z}}_e, \hat{\mathbf{z}}_e, \hat{\mathbf{z}}_e] \tag{24}$$

The solution to Eq. (23) with Eq. (24) as a "secondary task", [24], is given by Eq. (25) where the (+) superscript indicates the generalized inverse. For brevity let $\mathbf{J}_{L\psi}{}^t$ be indicated by $\mathbf{A}$ and let $\left(\nabla E - \mathbf{J}_{x\psi}{}^t \mathbf{w}_e\right)$ be indicated by $\mathbf{b}$. The vector $\boldsymbol{\eta} \in \Re^3$ is chosen so that $\boldsymbol{\tau}$ satisfies Eq. (24).

$$\boldsymbol{\tau} = \mathbf{A}^+\mathbf{b} + \left(\mathbf{I} - \mathbf{A}^+\mathbf{A}\right)\boldsymbol{\eta} \tag{25}$$

$$\boldsymbol{\eta} = \left(\mathbf{Z}_e\left(\mathbf{I} - \mathbf{A}^+\mathbf{A}\right)\right)^+\left(-\mathbf{f}_e - \mathbf{Z}_e\mathbf{A}^+\mathbf{b}\right) \tag{26}$$

This redundancy resolution presents one possible way to control the load sharing between the backbones while reducing the risk of buckling of the primary backbone. However, it does not necessarily constitute an optimal solution in which the load sharing among all the backbones (secondary and primary) is fulfilled. An actuation unit is being designed to actuate the snake-like unit using this solution or other optimal solutions that are sought as part of our future work.

VIII. Prototype Experiment

A first prototype of the snake unit is shown in Fig. 6. The length of the snake unit is 28 mm and its diameter is 4.2 mm. It is designed to bend ±90° in any direction. The primary and secondary backbones are made of super elastic NiTi tubes having 0.66 and 0.5 mm external and internal diameters. All the disks have a diameter of 4.2 mm and 1.6 mm thickness. The unit of Fig. 6 was manually actuated by two out of three existing secondary backbones and was able to apply more than 1 newton at its tip. In the design we followed a design goal such that the strain in the tubes does not exceed 4%. This strain limit is used to prevent degradation of the superelastic properties of the tubes over continuous operation. Once the actuation unit is built, it will be actuated using the three secondary backbones and by doing so it will demonstrate better load sharing among the backbones and thus we will be able to bend it further without violating the strain limit. This prototype serves as an experimental setup for determining fatigue resilience and additional design parameters such as the maximal distance between the spacer disks to prevent buckling.

The unit of Fig. 6 demonstrated some bending nonlinearity which can be seen in Fig. 6-b. We suspect it stems from extra loose tolerances of the passages in the base disk. These passages allow the secondary backbones to pass through the

base and are supposed to provide only axial motion capability, but in the existing model they allow small angular motion capability due to the tolerances. Another possible explanation for this behavior is the fact that we are using only two backbones out of three and by doing so we are loading the tubes such that their extension becomes non-negligible. These hypotheses remain to be verified in our future work.

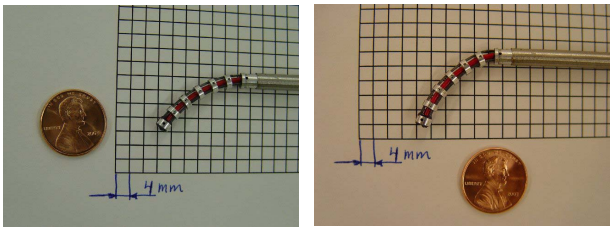

(a) (b)

Fig. 6 The 4.2 mm diameter prototype in two bent configurations with only two of the available three secondary backbones actuated manually.

IX. CONCLOSION

This paper presented our up-to-date work on designing a high dexterity, high accuracy slave for tele-operated minimally invasive surgery of the throat. The slave is a 34 DoF unit capable of simultaneously manipulating up to three surgical tools. This system is designed to allow tissue reconstruction of the vocal folds and suturing tasks - currently extremely difficult to perform in a minimally invasive approach.

The main unit of this slave is an eleven DoF distal dexterity unit composed from a snake-like unit and a detachable parallel wrist that provides surgical tool exchangeability. The design of the snake-like unit was presented. This unit uses multiple superelastic tubes as flexible backbones actuated in push-pull modes. This design provides future downsize scalability and manufacturing simplicity.

Finally, the paper outlined the kinematic analysis guiding our design. The paper suggested using the available actuation redundancy in the snake-like unit to minimize the risk of buckling of the primary backbone. One possible redundancy resolution achieving this goal was presented. Finally, an early experiment with a first built prototype was shown.

ACKNOWLEDGEMENTS

This work was partially funded by the National Science Foundation (NSF) under Engineering Research Center grant #EEC9731478, NSF grant #IIS9801684, and by the Johns Hopkins University internal funds.

REFERENCES

[1] R. Taylor, J. Funda, B. Eldridge, S. Gomory, K. Gurben, D. LaRose, M. Talamini, L. Kavoussi, J. Anderson, "A Telerobotics Assistant for Laproscopic Surgery," IEEE Engineering in Medicine and Biology Magazine, 14(3), pp. 279-288, 1995.

[2] G.S. Guthart, J.K. Salisbury, "The Intuitive™ Telesurgery System: Overview and Application," *ICRA*'2000, pp. 618-621, 2000.

[3] J. M. Sackier and Y. Wang, "Robotically assisted laprascopic surgery from concept to development," Surgical Endoscopy, Vol. 8, pp. 63-66, 1994.

[4] M. Shoham, M. Burman, E. Zehavi, L. Joskowicz, E. Batkilin, Y. Kunicher, "Bone-Mounted Miniature Robot for Surgical Procedures: Concept and Clinical Applications," IEEE Trans. Robot. Automat., Vol. 19, No. 5, pp. 893-901, 2003.

[5] N. Simaan, M. Shoham, "Robot Construction for Surgical Applications." The First IFAC Conference on Mechatronic Systems, Darmstadt, Germany, September 18-20, 2000.

[6] R.H. Taylor, D. Stianovici, "Medical Robotics in Computer-Integrated Surgery," IEEE Trans. Robot. Automat., Vol. 19, No. 5, pp. 765-781, 2003.

[7] M. Cavusoglu, I. Villanueva, F. Tendick, 2001, "Workspace Analysis of Robotics Manipulators for a Teleoperated Suturing Task," IEEE/RSJ International Conference on Intellegent Robots and Systems (IROS2001), Maui, HI.

[8] Y. Nakamura, A. Matsui, T. Saito, K. Yoshimoto, "Shape-Memory-Alloy Active Forceps for Laparoscopic Surgery," *ICRA*'95, pp. 2320-2327, 1995.

[9] P. Dario, C. Paggetti, N. Troisfontaine, E. Papa, T. Ciucci, M.C. Carrozza, M. Marcacci, "A Miniature Steerable End-Effector for Application in an Integrated System for Computer-Assisted Arthroscopy", *ICRA*'97, pp. 1573-1579, 1997.

[10] D. Reynaerts, J. Peirs, H. Van Brussel, "Shape memory micro-actuation for a gastro-intesteinal intervention system," Sensors and Actuators, Vol. 77, pp. 157-166, 1999.

[11] J. Piers, D. Reynaerts, H. Van Brussel, G. De Gersem, H.T. Tang, "Design of an Advanced Tool Guiding System for Robotic Surgery," *ICRA*'2003, pp. 2651-2656, 2003.

[12] L. Adhami, E.C. Maniere, "Optimal Planning for Minimally Invasive Surgical Robots," IEEE Trans. Robot. Automat., Vol. 19, No. 5, pp. 854-863, 2003.

[13] S. Hirose, S. Ma, "Coupled Tendon-Driven Multijoint Manipulator", Proc. *ICRA*'91, pp.1268-1275, 1991.

[14] G., Chirikjian, J. Burdick, "Design and Experiments with a 30 DOF Robot," *ICRA*'93, pp. 113-119, 1993.

[15] E. Paljug, T. Ohm, S. Hayati, "The JPL Serpentine Robot: a 12 DOF System for Inspection," *ICRA*'95, pp. 3143-3148, 1995.

[16] I. Walker, M. Hannan, "A Novel "Elephant's Trunk" Robot". Proceedings of the 1999 IEEE/ASME International Conference on Advanced Intelligent Mechatronics, pp. 410-415, 1999.

[17] I. Ebert-Uphoff, G. Chirikjian, "Inverse Kinematics of Discretely Actuated Hyper-Redundant Manipulators Using Workspace Densities", *ICRA*'96,pp. 139-145, 1996.

[18] J. Suthakorn, G.S. Chirikjian, "A New Inverse Kinematics Algorithm for Binary Manipulators with Many Actuators" Advanced Robotics, pp 225-244, Vol. 15, No. 2, 2001.

[19] I.A. Gravange, I.D. Wlaker,"Kinematic Transformations for Remotely-Actuated Planar Continuum Robots," *ICRA*'2000, pp. 19-26, 2000.

[20] C. Li, C. Rhan, "Design of Continuous Backbone, Cable-Driven Robots," ASME J. of Mechanical Design, Vol. 124, pp., 265-271, 2002.

[21] P. Breedveld, International Patent application, International Publication Number WO 01/10292 A1, Applicant: Delft University of Technology, Priority date 06/08/1999, 2000.

[22] S. Hirose, Biologically Inspired Robots, Snake-Like Locomotors and Manipulators, Oxford University Press, section 10.3, pp. 147-154, 1993.

[23] G. Immega, K. Antonelli, "The KSI Tentacle Manipulator," *ICRA*'95, pp. 3149-3154, 1995.

[24] T. Yoshikawa, *Foundations of Robotic Analysis and contol*, The MIT Press, 1990.